Exosome-encapsulated miR-26a attenuates aldosterone-induced tubulointerstitial fibrosis by inhibiting the CTGF/SMAD3 signaling pathway

HUI ZHENG*, JIALING JI*, TANGMING ZHAO, E WANG and AIQING ZHANG

Department of Pediatric Nephrology, The Second Affiliated Hospital of Nanjing Medical University, Nanjing, Jiangsu 210003, P.R. China

Received August 1, 2022; Accepted November 10, 2022

DOI: 10.3892/ijmm.2022.5214

Abstract. Renal tubulointerstitial fibrosis (TIF) is a hallmark in the continuous progression of chronic kidney disease (CKD), in which excessive activation of the renin-angiotensin-aldosterone system serves a crucial role. Currently, there are no targeted therapies for the progression of TIF. microRNA (miR)-26a may be an ideal anti-fibrosis candidate molecule; however, the effect of miR-26 on aldosterone (ALD)-induced TIF remains unclear. This study aimed to elucidate the role of miR-26a in ALD-induced TIF. In the present study, we hypothesized that delivery of miR-26a by exosomes could attenuate ALD-induced TIF. miR-26a expression was downregulated in the kidney of ALD-induced mice compared with the mice in the sham group. Exosome-encapsulated miR-26a (Exo-miR-26a) was manufactured and injected into ALD-treated mice through the tail vein. *In vivo* experiments showed that Exo-miR-26a alleviated the downregulated miR-26a expression in the kidney, tubular injury and ALD-induced TIF, which was determined using Masson's trichrome staining and assessment of lipocalin 2, α-smooth muscle actin, collagen I and fibronectin expression. Moreover, *in vitro* experiments revealed that Exo-miR-26a inhibited epithelial-mesenchymal transition and extracellular matrix deposition in mouse tubular epithelial cells. Mechanistically, overexpressing miR-26a led to decreased expression levels of connective tissue growth factor by directly binding to its 3'-UTR and inhibiting the activation of SMAD3. These findings demonstrated that the exosomal delivery of miR-26a may alleviate ALD-induced TIF, which may provide new insights into the treatment of CKD.

Correspondence to: Dr Aiqing Zhang, Department of Pediatric Nephrology, The Second Affiliated Hospital of Nanjing Medical University, 262 Zhongshan North Road, Nanjing, Jiangsu 210003, P.R. China
E-mail: njaiqing@njmu.edu.cn

*Contributed equally

Abbreviations: α-SMA, α-smooth muscle actin; ALD, aldosterone; CKD, chronic kidney disease; CTGF, connective tissue growth factor; ECM, extracellular matrix; EMT, epithelial-mesenchymal transition; Exo, exosome encapsulated; LCN2, lipocalin 2; mTEC, mouse tubular epithelial cells; NC, negative control; oe-, overexpression; TIF, tubulointerstitial fibrosis

Key words: exosomes, microRNA-26a, aldosterone, CTGF, SMAD3

Introduction

Chronic kidney disease (CKD) is a major public health problem worldwide (1). The global prevalence of CKD is 9.1% (1), with rates up to 15% in the USA and 9.2% in China (2,3), causing a high economic burden. Renal tubulointerstitial fibrosis (TIF) is considered a common stage in the progression of CKD to end-stage renal disease; it is accompanied by inflammatory cell infiltration and excessive deposition of extracellular matrix (ECM) in the renal interstitium (4). Moreover, excessive activation of the renin-angiotensin-aldosterone system (RAAS) results in glomerular sclerosis and TIF, serving a pivotal role in CKD progression (5). Aldosterone (ALD) can affect the renal system and contribute to tissue inflammation, injury, glomerulosclerosis and interstitial fibrosis (6). Our previous studies have shown that increased ALD levels promote podocyte damage, glomerular sclerosis, renal tubular epithelial cell damage, renal interstitial inflammation and fibrosis (7-9). At present, the treatments for TIF, such as renal replacement therapy, dialysis and kidney transplantation, are limited.

MicroRNAs (miRNAs) are highly conserved, endogenous, single-stranded non-coding RNA molecules with a length of ~22 nt, which can regulate target genes expression by degrading mRNAs or inhibiting post-transcriptional translation (10). Moreover, >30% of protein expression in mammals is regulated by miRNAs, including that of most kidney fibrosis-related proteins (11). A number of studies have demonstrated that several miRNAs, including miR-21, miR-26, miR-29, miR-141 and miR-200, are associated with renal fibrotic processes (12,13). Our previous study has shown that miR-26a exerts an antifibrotic effect in obstructive kidney disease (14). Additionally, miR-26a serves a considerable role in angiotensin-II-induced cardiac fibrosis (15). Moreover, it has been confirmed that miR-26a is downregulated in fibrotic

diseases of the lung, lens and liver (16-18). These data suggest that miR-26a could act as an ideal anti-fibrosis candidate molecule. However, the effect of miR-26a on ALD-induced TIF remains unclear. Moreover, circulating miRNAs are extremely unstable and can be easily degraded by ribonucleases in the plasma (19). Coupled with the complex structure of the kidney, whose damage can lead to functional problems, and the variety of kidney cells, whose morphology, gene expressions and physiological functions varies, the lack of high-efficiency media to introduce miRNAs into the kidney cells is a bottleneck that is difficult to overcome in this field (20-22). Thus, it is important to identify new, safe and efficient gene therapy vectors for TIF.

Exosomes are cup-shaped microvesicles with a diameter of ~30-100 nm that are secreted by almost all cell types (23). Exosomes are found in blood, cerebrospinal fluid, urine and other body fluids; they deliver proteins, miRNAs, long non-coding RNAs and mRNAs produced by cells in different states throughout the body (24). In recent years, exosomes have received extensive attention owing to their role in communication between cells and tissues (25). The various mechanisms involved in exosome biogenesis affect the content of exosomes, including various receptors, proteins, genetic materials (DNA, mRNAs and miRNA) and lipids to target cells (23). Furthermore, exosomes derived from human endothelial cells deliver miR-486 to the kidneys to reduce ischemic kidney injury (26). Thus, an exosome encapsulation-based miRNA delivery system may be an attractive candidate for manipulating miR-26a for treating TIF in CKD (14).

In the present study, we hypothesized that the exogenous delivery of exosome encapsulated (Exo)-miR-26a to injured kidneys could ameliorate ALD-induced TIF. Moreover, results from the current study may provide a basis for not only clinical research on the mechanism of TIF in CKD but also the use of exosomes for the treatment of CKD.

Materials and methods

Generation and isolation of exosomes with miR-26a. When 293 cells (cat. no. CL-0005; Procell Life Science &Technology Co., Ltd.) grew to 60-70% confluence, they were transfected with miR-26a or empty vector adenoviruses (ADV1-U6-GFP-mmu-miR-26a and ADV1-NC, respectively; Shanghai GenePharma Co., Ltd.). The 293 cells were cultured in serum-free DMEM containing 0.1% DiD far-red plasma membrane fluorescent probe (cat. no. C1039; Beyotime Institute of Biotechnology) at 37˚C for 20 min. After washed by PBS, the 293 cells were cultured in DMEM containing 10% FBS and miR-26a or empty vector adenoviruses (final titer $1x10^6$ PFU/ml), and the exosomes were allowed to be secreted at 37˚C for 48 h. The supernatant of the cell culture medium was then collected and centrifuged at 2,000 x g at 4˚C for 20 min. The supernatant was collected and centrifuged again at 13,500 x g at 4˚C for 20 min. The supernatant was harvested and centrifuged at 200,000 x g at 4˚C for 2 h. Finally, the miR-26a enriched exosomes and empty vector exosomes were resuspended in PBS. The morphology and size of the exosomes were analyzed using transmission electron microscopy (TEM). The identity of the exosomes was confirmed by western blot analysis of exosomal marker proteins CD63, CD81 and Alix, as described below. Mice were injected with exosomes through the caudal vein, as described below; at the end of the study, kidneys were excised, and fluorescence images were captured using the IVIS Spectrum *in vivo* Image System (PerkinElmer, Inc.).

TEM. The exosome pellets were re-suspended in 50 μl 2% paraformaldehyde (density $4.9x10^7$ particles/ml), and 5 μl of the suspension was placed on a sheet of parafilm. A carbon-coated copper grid was floated on the drop for 20 min at room temperature. The grid was washed by PBS for 3 min twice and excess liquid was drained by touching the grid edge against a piece of clean filter paper. The grid was placed in 1% glutaraldehyde at room temperature for 5 min. The grid was stained with uranyl acetate (UA) dye solution with pH 7.0 at room temperature for 10 min, and then coated in a methyl cellulose-UA suspension on ice for 10 min. The grid was removed and excess liquid was drained off. The grid was allowed to dry at room temperature for 5-10 min and then observed under the electron microscopy at 80 kilo electron volts.

Animal model. Male C57BL/6J mice (n=20; age 6-8 weeks; weight, 20-22 g) were purchased from the Beijing Vital River Laboratory Animal Technology Co., Ltd., housed with five mice per cage and maintained at 19-21˚C on a 12-h light/dark cycle with free access to food and water. Following 1 week of adaptive feeding, an osmotic mini-pump was implanted subcutaneously in the interscapular region to administer 1X PBS (100 μl) or ALD (100 μl at 0.75 μg/h) after mice were anesthetized using intraperitoneal (i.p.) injection with the 50 mg/kg 1% pentobarbital sodium. Subsequently, the mice were randomly divided into four groups (n=5 mice/group): i) sham group; ii) ALD group; iii) ALD + Exo-negative control (NC) group; and iv) ALD + Exo-miR-26a group. All mice were given 1% NaCl drinking water throughout the experimental period. The ALD + Exo-miR-26a group mice received 100 μg Exo-miR-26a or Exo-NC injected into the tail vein every 7 days starting the day the mini-pump was implanted. At the end of the 28-day infusion period, all mice were anaesthetized using 50 mg/kg 1% pentobarbital sodium and euthanized by i.p. injection of pentobarbital sodium (100 mg/kg). Death was confirmed by the following criteria: Respiratory arrest, cardiac arrest, dilation of the pupils and disappearance of nerve reflex. The mice were placed in a metabolic cage for 24 h before euthanasia to obtain urine samples. A total of 100 μl blood was collected from the orbital venous sinus of anesthetized mice, prior to euthanasia, at the Animal Experiment Center of Nanjing Medical University. Kidneys were harvested after mice were sacrificed. The study protocols were reviewed and approved by the Institutional Animal Care and Use Committee of Nanjing Medical University (ref. no. IACUC-2107049).

Cell culture. Mouse tubular epithelial cells (mTECs; cat. no. CRL-3361) were purchased from the American Type Culture Collection and cultured in DMEM containing 10% FBS and 5 mM glucose at 37˚C and 5% CO_2. To determine the effects of ALD on mTECs, cells were divided into control and ALD groups; equal numbers ($0.3x10^6$ cells) of growth-arrested mTECs (preincubated in serum-free DMEM for 6 h) were

incubated in medium (with 10% FBS) containing either PBS (control) or ALD ($1x10^{-6}$ M) at 37˚C for 48 h when the density reached 60-70%. Cells were harvested at the end of the incubation period for further experiments. 293 cells were cultured in DMEM containing 10% FBS and 25 mM glucose at 37˚C and 5% CO_2; 293 cells were used for exosome production and luciferase binding experiments.

Reverse transcription-quantitative PCR (RT-qPCR). To measure miRNA or mRNA expression levels, total RNA was extracted from the kidney tissue (10 mg) and mTECs ($1x10^6$ cells) using TRIzol® reagent (Invitrogen; Thermo Fisher Scientific, Inc.) For miR-26a, 1,000 ng of total RNA enriched in small RNAs was reverse transcribed using the All-in-One MicroRNA Assay kit (iGene Biotechnology Co., Inc.). The mouse U6 gene was used as the loading control. For mRNA expression, cDNA was synthesized using HIScript III RT SuperMix (Vazyme Biotech Co., Ltd.); β-actin was used as an internal reference. All primers were purchased from GeneRay Biotech Co., Ltd. Primer sequences are listed in Table I; a reverse primer was used for miR-26a. miRNA and mRNA expression levels were calculated as the difference between the threshold values of the control and experimental genes using the $2^{-\Delta\Delta cq}$ method (27).

Table I. Primer sequences used for reverse transcription-quantitative PCR.

Gene	Primer sequence (5'-3')
β-actin	F: CATCCGTAAAGACCTCTATGCCAAC
	R: ATGGAGCCACCGATCCACA
Collagen I	F: GTCAGACCTGTGTGTTCCCTACTCA
	R: TCTCTCCAAACCAGACGTGCTTC
α-SMA	F: CAGCAAACAGGAATACGACGAA
	R: AACCACGAGTAACAAATCAAAGC
LCN2	F: GCCCTGAGTGTCATGTGTCT
	R: GAACTGATCGCTCCGGAAGT
CTGF	F: GGGCCTCTTCTGCGATTTC
	R: ATCCAGGCAAGTGCATTGGTA
miR-26a	F: ACACTCCAGCTGGGTTCAAGTAATC CAGGA
	R: TGGTGTCGTGGAGTCG
U6	F: CTCGCTTCGGCAGCACATATACT
	R: ACGCTTCACGAATTTGCGTGTC

α-SMA, α-smooth muscle actin; CTGF, connective tissue growth factor; LCN2, lipocalin 2; miR, microRNA.

Western blot. Western blot was performed as described previously (14). RIPA lysis buffer (cat. no. P0013B; Beyotime Institute of Biotechnology) and PMSF protease inhibitor (cat. no. ST506; Beyotime Institute of Biotechnology) were added to the kidney tissue (10 mg; crushed using a tissue grinder) and mTECs ($1x10^6$ cells) at a ratio of 100:1. The suspension was placed on ice, and tissues and cells were lysed for 1 h. The suspension was centrifuged at 12,000 x g at 4˚C for 30 min. The supernatant was collected, and the protein concentration was then measured using enhanced BCA protein assay kit (cat. no. P0010; Beyotime Institute of Biotechnology). Proteins (50 μg) were separated by 10% SDS-PAGE and transferred to PVDF membranes (MilliporeSigma; cat. no. HATF09025). The PVDF membranes were incubated with the primary antibodies at 4˚C overnight; the primary antibodies (all 1:1,000) used are as follows: Anti-α-smooth muscle actin (α-SMA; cat. no. BF9212; Affinity Biosciences, Ltd.), collagen I (cat. no. ab34710; Abcam), connective tissue growth factor (CTGF; cat. no. ab6992; Abcam), lipocalin 2 (LCN2; cat. no. DF6816; Affinity Biosciences, Ltd.), E-cadherin (cat. no. AF0131; Affinity Biosciences, Ltd.), SMAD3 (cat. no. AF6362; Affinity Biosciences, Ltd.), phosphorylated (p)-SMAD3 (cat. no. AF3362; Affinity Biosciences, Ltd.), CD63 (cat. no. sc5275, Santa Cruz Biotechnology, Inc.), CD81 (cat. no. P35762; Cell Signaling Technology, Inc.), Alix (cat. no. sc53540; Santa Cruz Biotechnology, Inc.), β-tubulin (cat. no. T0023; Affinity Biosciences, Ltd.) and GAPDH (cat. no. T0004; Affinity Biosciences, Ltd.). The PVDF membranes were incubated with the secondary antibodies at room temperature for 1 h; the secondary antibodies (all 1:2,000) used were: HRP-conjugated goat anti-mouse (cat. no. L3032; Signalway Antibody LLC) and HRP-conjugated goat anti-rabbit (cat. no. L3012; Signalway Antibody LLC). Protein bands were visualized using an enhanced chemiluminescence reagent (Immobilon Western HRP Substrate; cat. no. WBKLS0100; Merck KGaA) and a gel imaging analysis system. ImageJ software 1.8.0 (National Institutes of Health) was used to semi-quantify expression of proteins normalized to GAPDH or β-tubulin.

Cell transfection. The miR-26a mimic, miR-26a inhibitor, CTGF small interfering (si)RNA, CTGF overexpression (oe) plasmids [pEX-3(pGCMV/MCS/Neo)], and their respective NCs were obtained from Shanghai GenePharma Co., Ltd.; the sequences are listed in Table II. mTECs or 293 cells were maintained in 6- or 12-well plates before transfection. When the cell density reached 30-50%, they were transfected with Lipofectamine® 2000 (cat. no. 11668019; Thermo Fisher Scientific, Inc.) according to the manufacturer's instructions. For the co-transfection of oe-CTGF plasmids and miR-26a mimic (or si-CTGF and miR-26a inhibitor), plasmids (100 ng) and miR-26a mimic (20 μM), si-CTGF (20 μM) or miR-26a inhibitor (20 μM) were used in serum-reduced medium (Opti-MEM). The cells were incubated with the mimic or inhibitor (final concentration 50 nM)/Lipofectamine mixture at 37˚C for 6 h, and then the Opti-MEM medium was replaced with a complete medium. For single transfections, oe-CTGF plasmids (100 ng), miR-26a mimic (20 μM), si-CTGF (20 μM) or miR-26a inhibitor (20 μM) was used in serum-reduced medium (Opti-MEM). The cells were incubated with the mimic (or inhibitor or si-CTGF or plasmids)/Lipofectamine mixture at 37˚C for 6 h, and then the Opti-MEM medium was replaced with a complete medium. After 24-48 h, cells were collected for further analysis. The viability of cells after treating with siRNA and inhibitors is presented in Fig. S1.

Masson's trichrome staining. Fresh kidney tissue was fixed in 4% paraformaldehyde at room temperature for 24 h, then

Table II. Sequences of the RNA oligonucleotides used for cell transfection.

Name	Sequence (5'-3')
miR-26a mimic	Sense: UUCAAGUAAUCCAGGAUAG GCU Antisense: CCUAUCCUGGAUUACU UGAAUU
NC mimic	Sense: UUCUCCGAACGUGUCACG UTT Antisense: ACGUGACACGUUCGG AGA ATT
miR-26a inhibitor	Sense: AGCCUAUCCUGGAUUACUU GAA
NC inhibitor	Sense: CAGUACUUUUGUGUAGUA CAA
CTGF siRNA	Sense: CCCUGUACUACAGGAAGA UTT Antisense: AUCUUCCUGUAGUAC AGGGTT

CTGF, connective tissue growth factor; miR, microRNA; NC, negative control; si, small interfering RNA.

soaked in 75% ethanol overnight. The tissues were dehydrated in an ascending ethanol gradient. Then, the tissues were cleared with xylene, and the transparent tissues were immersed in paraffin; the embedded wax blocks were subsequently sectioned to a thickness of 3 μm. After the sections were straightened and flattened in a 40˚C water bath, they were collected by anti-slip slides and baked at 65˚C overnight. The sections were stained with hematoxylin at room temperature for 5-10 min and rinsed with water. The tissues were differentiated with an ethanol hydrochloric acid differentiation solution and stained with vincristine 3R at room temperature for 5-10 min. Next, the sections were immersed in 1% phosphomolybdate solution for about 5 min at room temperature until the collagen fibers or background were colorless and the myelin sheath was red. Sections were then counterstained with aniline blue for 5 min at room temperature, soaked in 1% acetic acid at room temperature for 1 min, and then dehydrated with 95% ethanol. The sections were dehydrated with absolute ethanol, cleared with xylene for 10 min at room temperature, and sealed with neutral resin. Finally, the sections were observed under an inverted light microscope.

Immunofluorescence. Paraffin-embedded sections of the mouse kidney were prepared as aforementioned. After baking at 65˚C for 2 h, the sections were dewaxed in xylene I (20 min) and xylene II (20 min) at room temperature, and then rehydrated through a descending series of ethanol solutions (100-70%) at room temperature for 5 min respectively. Antigen retrieval was followed by boiling in citrate buffer and cooling to room temperature. After blocking with 5% BSA (cat. no. 4240; Guangzhou Saiguo Biotech Co., Ltd.) for 1 h, the primary antibody was added dropwise, and the sections were incubated at 4˚C overnight. Sections were then stained with secondary antibodies for 1 h at room temperature, and the nuclei were labeled with DAPI at room temperature for 10 min. The sections in NC group were only incubated with secondary antibodies. The primary antibodies (all 1:200 in 1% BSA) used were: Anti-E-cadherin (cat. no. AF0131; Affinity Biosciences, Ltd.), anti-fibronectin (cat. no. AF5335; Affinity Biosciences, Ltd.), anti-α-SMA (cat. no. BF9212; Affinity Biosciences, Ltd.); and the secondary antibodies (all 1:500, diluted with 1%BSA) used were: Alexa Fluor 647-conjugated goat anti-mouse IgG (cat. no. S0014; Affinity Biosciences, Ltd.) and Alexa Fluor® 488- conjugated goat anti-rabbit IgG (cat. no. ab150077; Abcam). After sealing the tissues with coverslips and an antifade mounting medium (cat. no. P0126; Beyotime Institute of Biotechnology), the sections were observed under a fluorescence microscope.

Luciferase reporter assay. Previous studies have confirmed that CTGF is the downstream target of miR-26a (14,15,28); thus, the targeting relationship between them was verified in the present study. As CTGF was a predicted target of miR-26a, luciferase reporter constructs in which the luciferase coding sequence was fused to the 3'-UTRs of CTGF (pLuc.miR-26a-CTGF-3'-UTR) were generated by Shanghai GenePharma Co., Ltd. The wild-type (WT; 100 ng) or mutant (MUT; 100 ng) plasmids were co-transfected with NC mimic (20 μM) or miR-26a mimic (20 μM) into 293 with Lipofectamine 2000 transfection reagent when the cells reached 30-50% density ($0.1x10^6$ cells). After transfection at 37˚C for 48 h, the cells were harvested and lysed, and the luciferase activity was measured using a dual luciferase reporter gene assay kit (Shanghai GenePharma Co., Ltd.). Firefly luciferase activities were normalized to *Renilla* luciferase activities.

Cell Counting Kit-8 (CCK-8). Equal numbers of mTECs or 293 (5,000 cells/well) were inoculated into a 96-well plate and incubated in DMEM containing 10% FBS at 37˚C and 5% CO_2 for 24 h. siRNA (10 μl) and miR-26a inhibitors (50 nM) were added to the plate, and the cells were incubated at 37˚C and 5% CO_2 for 48 h. Subsequently, 10 μl of CCK-8 solution (cat. no. K1018; APExBIO Technology LLC) was added to each well, and the plate was incubated at 37˚C and 5% CO_2 for 1-4 h. The absorbance of the plate at 450 nm was measured using a microplate reader.

Serum creatinine (sCr) test. The collected blood was centrifuged at 956 x g at 4˚C for 10 min. The supernatant was harvested for the sCr test using a creatinine assay kit (sarcosine oxidase) (cat. no. C011-2-1; Nanjing Jiancheng Bioengineering Institute). A total of 6 μl serum (test group), creatinine standard (standard group) or ddH_2O (blank group) were added to individual wells of 96-well plate. Enzyme solution (180 μl) was then added to each well and the plate was then incubated at 37˚C for 5 min. The absorbance (A1) of the plate at 546 nm was then measured using a microplate reader. The plate was incubated at 37˚C for 5 min after adding 60 μl of enzyme solution B to each well, and the absorbance (A2) at 546 nm was measured again. The sCr content of samples were calculated according to the calculation formula in the protocol.

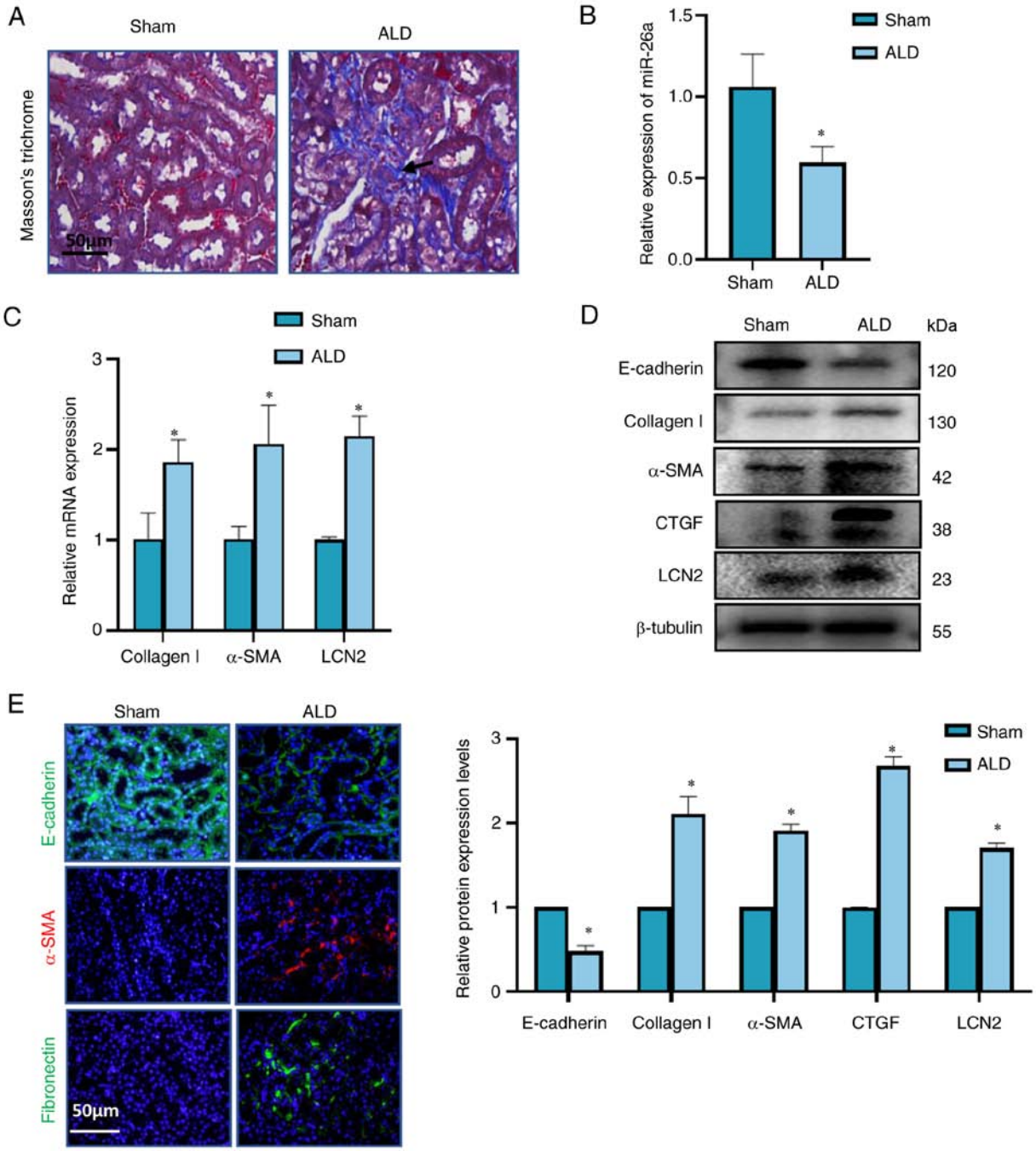

Figure 1. miR-26a expression is downregulated in the kidneys of ALD-induced mice. (A) Representative images of Masson's trichrome stained kidney tissues of mice in the sham and ALD groups. Scale bar, 50 μm. (B) RT-qPCR analysis of miR-26a expression levels in the kidney tissues of mice in the sham and ALD groups; U6 was used for normalization. (C) RT-qPCR analysis of collagen I, α-SMA and LCN2 mRNA expression levels in the kidney tissues of mice from the sham and ALD groups; β-actin was used for normalization. (D) Representative western blotting images and semi-quantitative analysis of E-cadherin, collagen I, α-SMA, CTGF and LCN2 protein expression levels in the kidney tissue of mice in the sham and ALD groups. (E) Immunohistochemical analysis of E-cadherin (green), α-SMA (red) and fibronectin (green) in the kidney tissue of mice in the sham and ALD groups; DAPI (blue) was used to stain the nuclei. Scale bar, 50 μm. Data are presented as the mean ± SD; n=5 mice/group; *P<0.05 vs. sham. α-SMA, α-smooth muscle actin2; CTGF, connective tissue growth factor; LCN2, lipocalin; RT-qPCR, reverse transcription-quantitative PCR.

Statistical analysis. Data are presented as the mean ± standard deviation of at least three independent experiments. Unpaired Student's t-test was used to compare two groups; one-way ANOVA followed by Tukey's post hoc test was used to compare the data from more than two groups. Statistical analyses were assessed with the SPSS v25 statistical software package (IBM Corp). P<0.05 was considered to indicate a statistically significant difference.

Results

miR-26a downregulation is associated with TIF in ALD-induced mice. To explore whether ALD can cause renal fibrosis, mice were randomly assigned to receive PBS or ALD treatment for 4 weeks. TIF was detected using Masson's trichrome staining, which showed obvious fibrosis in the ALD group (Fig. 1A). sCr levels were also higher in the ALD group

compared with levels in the sham group (Table III). Compared with the sham group, miR-26a expression levels were significantly reduced in the kidney tissue of mice in the ALD group (Fig. 1B). The mRNA expression levels of collagen I, α-SMA and the tubular injury marker LCN2 were higher in the kidney tissues of mice in the ALD group compared with levels in the sham group (Fig. 1C). Western blotting results revealed that ALD treatment increased the protein expression levels of collagen I, α-SMA, CTGF and LCN2 (Fig. 1D). Immunofluorescence results showed that the expression of α-SMA and fibronectin were notably increased in the kidneys of mice in the ALD group (Fig. 1E). Conversely, E-cadherin expression was lower in ALD-induced mice compared with the sham group (Fig. 1D and E). The immunofluorescence NC experiments shown in Fig. S2A demonstrate no notable difference between NC in Fig. S2A and the sham group in Fig. 1E. These results suggested that ALD-induced TIF may be related to reduced miR-26a expression levels.

Exo-miR-26a alleviates TIF in mice. To characterize the exosomes derived from 293 cells, their morphology and size were examined by TEM, which showed a lipid bilayer structure with a diameter of about 100 nm (Fig. 2A). The identity of the exosomes was confirmed by western blot analysis, which showed that the protein expression levels of the exosomal marker proteins CD63, CD81 and Alix in the 293-Exo group was increased compared with that in the 293-cell group, confirming that exosomes were harvested from the supernatant (Fig. 2B). Moreover, RT-qPCR analysis revealed that compared with that in the exosomes extracted from 293 cells transfected with the empty vector, the expression level of miR-26a in the exosomes of the Exo-miR-26a group was increased (Fig. 2C).

ALD-treated mice were injected with Exo-miR-26a or Exo-NC through the caudal vein. DiD fluorescence imaging results showed that the concentration of exosomes in the excised kidneys of mice injected with Exo-miR-26a was higher compared with that in the sham group, confirming that exosomes can deliver miR-26a into the kidneys (Fig. 2D). The results of RT-qPCR analysis showed that miR-26a expression levels in the kidneys of mice in the ALD + Exo-miR-26a group was significantly higher compared with that in the ALD and ALD + Exo-NC groups, whereas there was no significant difference between the ALD and ALD + Exo-NC groups (Fig. 2E).

Masson's trichrome staining was used to determine the degree of TIF. The results of the pathological examination of the mouse kidney sections indicated that collagen deposition in the renal interstitium of mice in the ALD + Exo-miR-26a group was reduced compared with that in the ALD group, whereas that in the ALD + Exo-NC group showed no difference with the ALD-only group (Fig. 2F). Compared with the ALD group, the sCr levels of the mice in the ALD + Exo-miR-26a group were significantly decreased, whereas those in the ALD + Exo-NC group was similar to that of the ALD group (Table III).

Moreover, the RT-qPCR results showed that the mRNA expression levels of collagen I, α-SMA and LCN2 in the kidney tissue of mice in the ALD + Exo-miR-26a group was decreased compared with that in the ALD and ALD + Exo-NC groups (Fig. 2G); no significant difference was detected between the ALD and ALD + Exo-NC groups (Fig. 2G).

Table III. sCr levels in ALD-induced model mice.

Group	sCr, μmol/l
Sham	17.09±6.95
ALD	58.49±11.81[a]
ALD + Exo-NC	57.06±12.75
ALD + Exo-miR-26a	30.24±11.19[b]

[a]P<0.05 vs. sham; [b]P<0.05 vs. ALD + Exo-NC ALD aldosterone; Exo, exosome-encapsulated; miR, microRNA; NC, negative control; sCr, serum creatinine.

Western blot analysis revealed that compared with the ALD and ALD + Exo-NC groups, the ALD + Exo-miR-26a group exhibited significantly lower expression levels of collagen I, α-SMA, CTGF and LCN2 in the kidneys (Fig. 2H). Immunofluorescence results showed that α-SMA and fibronectin expression levels were notably reduced in the ALD + Exo-miR-26a group compared with those in the ALD group (Fig. 2I), whereas E-cadherin expression showed the opposite trend (Fig. 2H and I). The immunofluorescence NCs are shown in Fig. S2B; there was no notable difference between NC in Fig. S2B and sham in Fig. 2I. These data suggested that miR-26a overexpression may reduce TIF in mice.

miR-26a overexpression alleviates ALD-induced epithelial-mesenchymal transition (EMT) and ECM deposition in mTECs. To explore whether ALD induces EMT and ECM deposition in mTECs, the cells were divided into two groups treated with either PBS or ALD for 48 h. The miR-26a expression level was determined by RT-qPCR, which revealed a decrease in the ALD group compared with the control (Fig. 3A). Moreover, the mRNA expression levels of collagen I, α-SMA and LCN2 in the control group were significantly lower compared with those in the ALD group (Fig. 3B). The results of western blot analysis revealed that collagen I, α-SMA, CTGF and LCN2 protein expression levels in the ALD group was upregulated compared with that in the control group, whereas the E-cadherin expression exhibited the opposite trend (Fig. 3C). Immunofluorescence results revealed that the α-SMA expression level in the ALD group was higher compared with that in the control group (Fig. 3G). These results suggested that ALD may induce EMT and ECM deposition in mTECs *in vitro*.

The role of miR-26a in EMT and ECM deposition was further investigated in mTECs treated with Exo-miR-26a. RT-qPCR results showed that the miR-26a expression levels were significantly increased in the ALD + Exo-miR-26a group compared with that in the ALD + Exo-NC group (Fig. 3D). Furthermore, the results from RT-qPCR and western blot analysis confirmed that compared with the ALD + Exo-NC group, Exo-miR-26a co-treatment inhibited the mRNA and protein expression levels, respectively, of collagen I, α-SMA, CTGF and LCN2 (Fig. 3E and F). However, E-cadherin protein expression level was higher in the ALD + Exo-miR-26a group compared with that in the ALD + Exo-NC group (Fig. 3F). The results of immunofluorescence showed that Exo-miR-26a

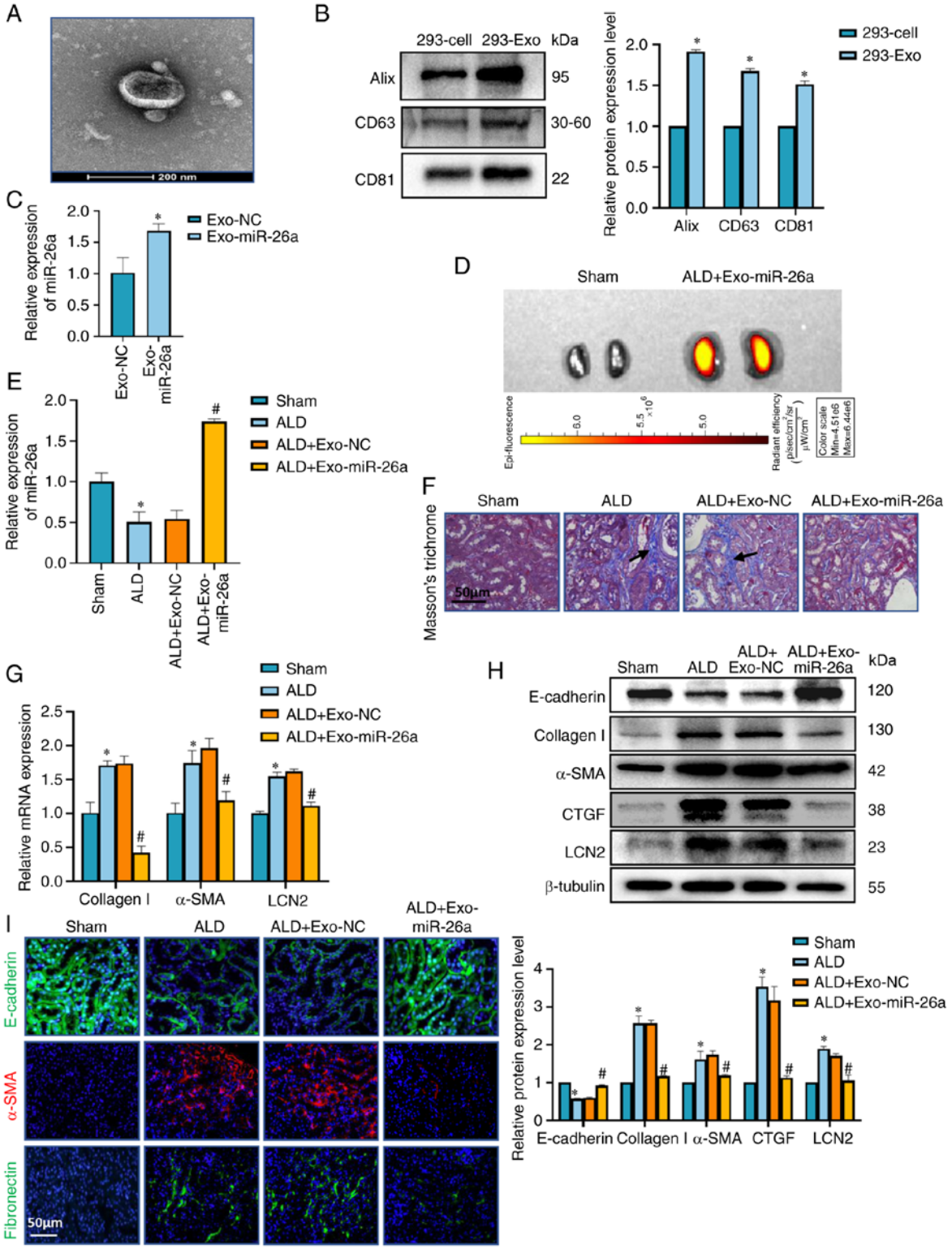

Figure 2. Exo-miR-26a alleviates ALD-induced renal fibrosis *in vivo*. (A) Transmission electron micrograph of exosomes extracted by ultra-high-speed differential centrifugation. Scale bar, 200 nm. (B) Representative western blotting images and semi-quantitative analysis of Alix, CD63 and CD81 protein levels in the exosomes. The protein of 293-cell group is the protein extracted from the adherent cells in the lower layer, the protein of 293-Exo group is the protein extracted from the exosomes isolated from the supernatant. (C) RT-qPCR analysis of miR-26a expression in the exosomes. Data are presented as the mean ± SD; *P<0.05 vs. Exo-NC. (D) DiD fluorescence imaging of exosomes in excised kidneys. The sham mice (left) were not injected and the ALD mice (right) were injected with exosomes through the caudal vein. (E) RT-qPCR analysis of miR-26a in the kidney of mice in the sham, ALD, ALD + Exo-NC and ALD + Exo-miR-26a groups; U6 was used for normalization. (F) Representative images of Masson's trichrome staining in the kidney tissues of mice in the different groups. Scale bar, 50 μm. (G) RT-qPCR analysis of collagen I, α-SMA and LCN2 mRNA expression levels in the kidney tissues of mice in the different groups; β-actin was used for normalization. (H) Representative western blotting images and semi-quantitative analysis of E-cadherin, collagen I, α-SMA, CTGF and LCN2 protein expression levels in the kidney tissues of mice from each group. Data are presented as the mean ± SD; n=5 mice/group; *P<0.05 vs. sham; #P<0.05 vs. ALD + Exo-NC. (I) Immunofluorescence analysis of E-cadherin (green), α-SMA (red) and fibronectin (green) in the kidney tissue of mice in the sham, ALD, ALD + Exo-NC and ALD + Exo-miR-26a groups; DAPI (blue) was used to stain the nuclei. Scale bar, 50 μm. α-SMA, α-smooth muscle actin; ALD, aldosterone; CTGF, connective tissue growth factor; Exo, exosome encapsulated; LCN2, lipocalin 2; miR, microRNA; NC, negative control; RT-qPCR, reverse transcription-quantitative PCR.

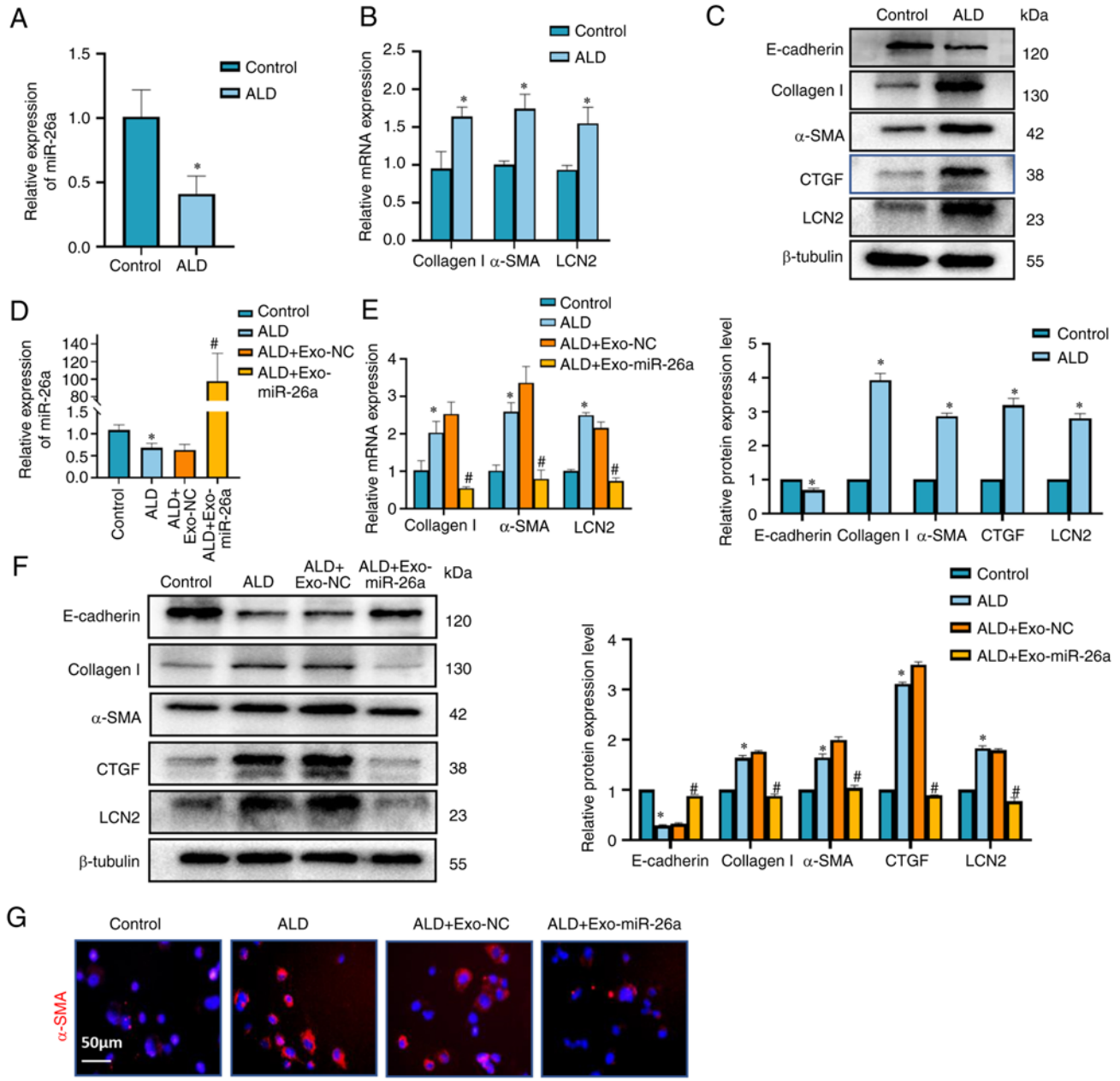

Figure 3. miR-26a overexpression alleviates ALD-induced EMT and ECM deposition in mTECs. RT-qPCR analysis of (A) miR-26a expression levels and (B) collagen I, α-SMA and LCN2 mRNA expression levels in mTECs treated with buffer (control) or ALD ($1x10^{-6}$ M) for 48 h. Results were normalized to β-actin. (C) Representative western blotting images and semi-quantitative analysis of E-cadherin, collagen I, α-SMA, CTGF and LCN2 protein expression levels in control- and ALD-treated mTECs. RT-qPCR analysis of (D) miR-26a expression and (E) collagen I, α-SMA and LCN2 mRNA expression levels in mTECs treated with buffer (control), ALD, ALD + Exo-NC and ALD + Exo-miR-26a. Results were normalized to β-actin. (F) Representative western blotting images and semi-quantitative analysis of E-cadherin, collagen I, α-SMA, CTGF and LCN2 protein expression levels in the variously treated mTECs. (G) Immunofluorescence analysis of α-SMA (red) in mTECs treated with buffer (control), ALD, ALD + Exo-NC or ALD+Exo-miR-26a; DAPI (blue) was used to stain the nuclei. Scale bar, 50 μm. Data are presented as the mean ± SD; *P<0.05 vs. Control; $^{\#}$P<0.05 vs. ALD + Exo-NC. A-SMA, α-smooth muscle actin; ALD, aldosterone; CTGF, connective tissue growth factor; ECM, extracellular matrix; EMT, epithelial-mesenchymal transition; Exo, exosome encapsulated; LCN2, lipocalin 2; miR, microRNA; mTEC, mouse tubular epithelial cells; NC, negative control; RT-qPCR, reverse transcription-quantitative PCR.

co-treatment notably decreased the expression of α-SMA in comparison with that in the ALD + Exo-NC group (Fig. 3G). The immunofluorescence NC shown in Fig. S2C indicates no difference compared with control group in Fig. 3G. Taken together, miR-26a overexpression reduced ALD-induced EMT and ECM deposition in mTECs.

miR-26a directly targets CTGF and negatively regulates its expression. Previous studies have confirmed that CTGF is the downstream target of miR-26a (14,15,28); the target site between miR-26a and 3'UTR of CTGF is shown in Fig. 4A, and it was verified using the luciferase reporter assay in 293 cells. Luciferase activity was decreased in response to co-transfection of miR-26a mimic and WT-CTGF-3'UTR, whereas no changes were observed in the cells treated with miR-26a mimic and MUT-CTGF-3'UTR (Fig. 4B). To further verify that miR-26a inhibits CTGF, miR-26a mimic or miR-26a inhibitor was co-transfected into 293 cells with

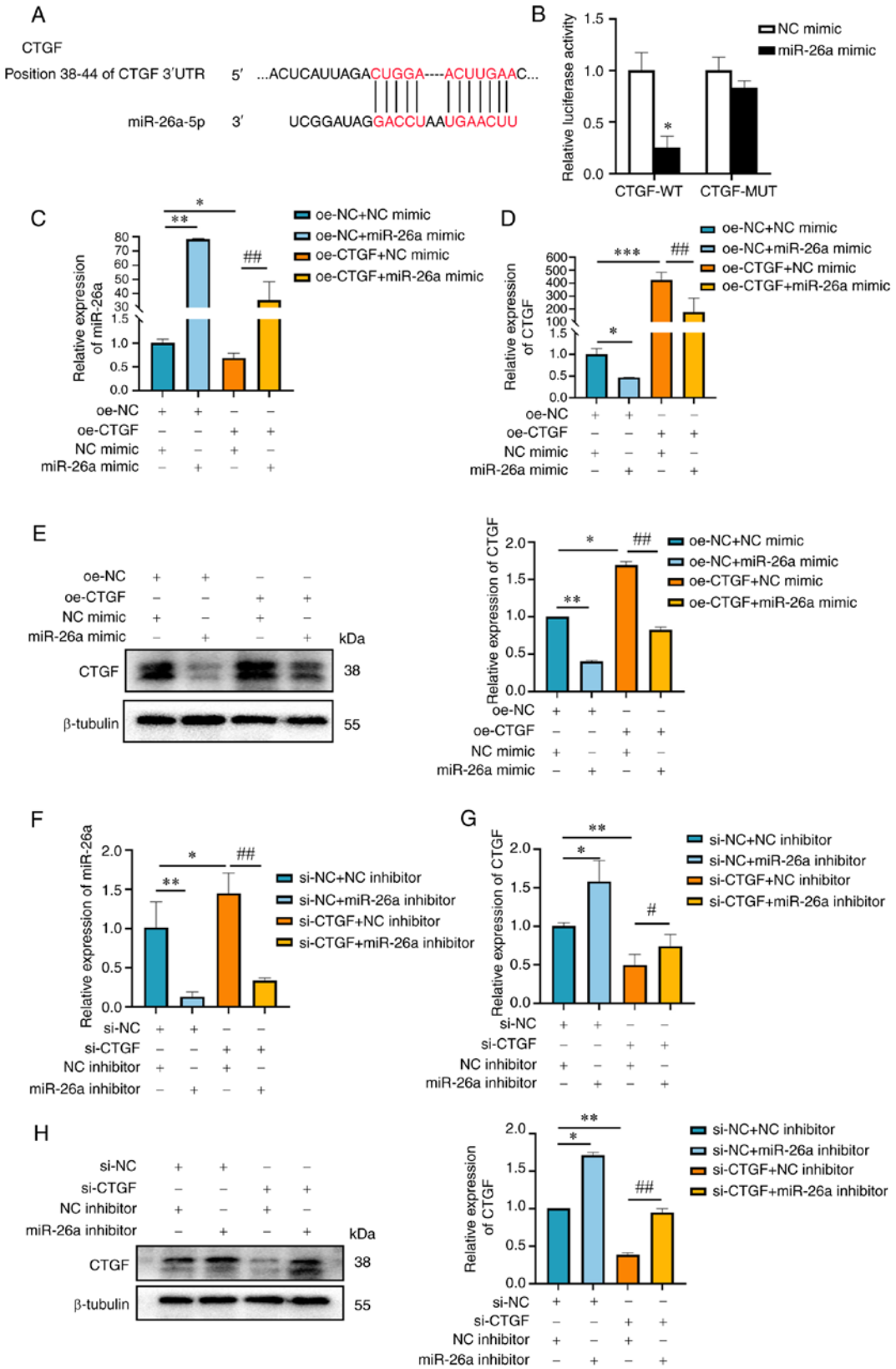

Figure 4. miR-26a directly targets CTGF and negatively regulates its expression. (A) miR-26a target site in the 3'UTR of CTGF. (B) Relative luciferase activity in 293 cells co-transfected with plasmids containing CTGF-WT or -Mut 3'-UTR and miR-26a mimic or NC mimic for 48 h. *P<0.05 vs. NC mimic. RT-qPCR analysis of (C) miR-26a expression and (D) CTGF mRNA expression levels in 293 cells co-transfected with oe-CTGF or oe-NC and miR-26a mimic or NC mimic. Results were normalized to U6 or β-actin, respectively. (E) Representative western blotting images and semi-quantitative analysis of CTGF protein expression levels in 293 cells co-transfected with oe-CTGF or oe-NC and miR-26a mimic or NC mimic. RT-qPCR analysis of (F) miR-26a expression and (G) CTGF mRNA expression levels in 293 cells co-transfected with si-CTGF or si-NC and miR-26a inhibitor or NC inhibitor. Results were normalized to U6 or β-actin, respectively. (H) Representative western blotting images and semi-quantitative analysis of CTGF protein levels in 293 cells co-transfected with si-CTGF or si-NC and miR-26a inhibitor or NC inhibitor. Data are presented as the mean ± SD; *P<0.05, **P<0.01, ***P<0.001; $^{\#}$P<0.05, $^{\#\#}$P<0.01. CTGF, connective tissue growth factor; miR, microRNA; Mut, mutant; NC, negative control; oe, overexpression; RT-qPCR, reverse transcription-quantitative PCR; si, small interfering RNA; UTR, untranslated region; WT, wild-type.

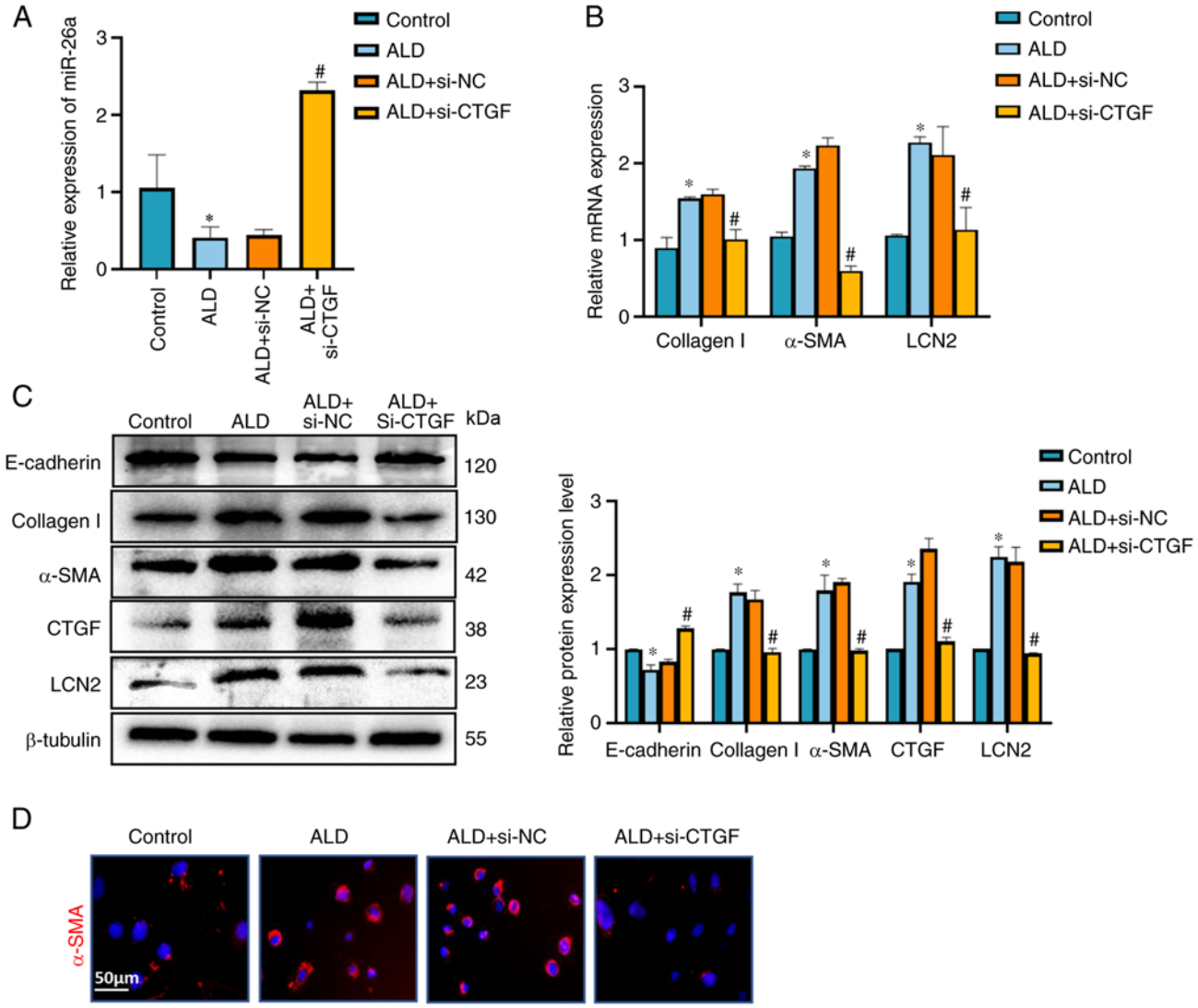

Figure 5. CTGF knockdown alleviates ALD-induced EMT and ECM deposition in mTECs. Cells were transfected with si-NC or si-CTGF for 6 h and then treated with ALD ($1x10^{-6}$ M) for 48 h. RT-qPCR analysis of (A) miR-26a expression and (B) collagen I, α-SMA and LCN2 mRNA expression levels in mTECs treated with buffer (control), ALD, ALD + si-NC or ALD + si-CTGF. Results were normalized to U6 or β-actin, respectively. (C) Representative western blotting images and semi-quantitative analysis of E-cadherin, collagen I, α-SMA, CTGF and LCN2 protein levels in the variously treated mTECs. (D) Immunofluorescence analysis of α-SMA (red) in the treated mTECs; DAPI (blue) was used to stain the nucleus. Scale bar, 50 μm. Data are presented as the mean ± SD; *P<0.05 vs. control, $^{\#}$P<0.05 vs. ALD + si-NC. α-SMA, α-smooth muscle actin; ALD, aldosterone; CTGF, connective tissue growth factor; ECM, extracellular matrix; EMT, epithelial-mesenchymal transition; LCN2, lipocalin 2; mTEC, mouse tubular epithelial cells; NC, negative control; RT-qPCR, reverse transcription-quantitative PCR; si, small interfering RNA.

oe-CTGF or CTGF siRNA, respectively, and the expression levels of miR-26a and CTGF were determined using RT-qPCR and western blot analysis. The results revealed a significant increase in miR-26a expression in oe-NC + miR-26a mimic group compared with oe-NC + NC mimic group, and in oe-CTGF + miR-26a mimic group compared with oe-CTGF + NC mimic group, whereas the miR-26a expression was decreased in oe-CTGF + NC mimic group compared with oe-NC + NC mimic group (Fig. 4C). RT-qPCR and western blotting analyses showed that the CTGF mRNA and protein expression levels, respectively, were decreased in the group transfected with oe-NC + miR-26a mimic compared with the group transfected with oe-NC + NC mimic, and in the group transfected with oe-CTGF + miR-26a mimic compared with the group transfected with oe-CTGF + NC mimic, whereas it was increased in the group transfected with oe-CTGF + NC mimic compared with the group transfected with oe-NC + NC mimic (Fig. 4D and E). Moreover, miR-26a expression was reduced in si-NC + miR-26a inhibitor group compared with si-NC + NC inhibitor group, and in si-CTGF + miR-26a inhibitor group compared with si-CTGF + NC inhibitor group, whereas it showed the opposite trend in si-CTGF + NC inhibitor group compared with si-NC + NC inhibitor group (Fig. 4F). CTGF mRNA and protein expression levels were upregulated in the group transfected with si-NC + miR-26a inhibitor compared with the group transfected with si-NC + NC inhibitor, and in the group transfected with si-CTGF + miR-26a inhibitor compared with the group transfected with si-CTGF + NC inhibitor, whereas it showed the opposite trend in the group transfected with si-CTGF + NC inhibitor compared with the group transfected with si-NC + NC inhibitor (Fig. 4G and H). These results further confirmed

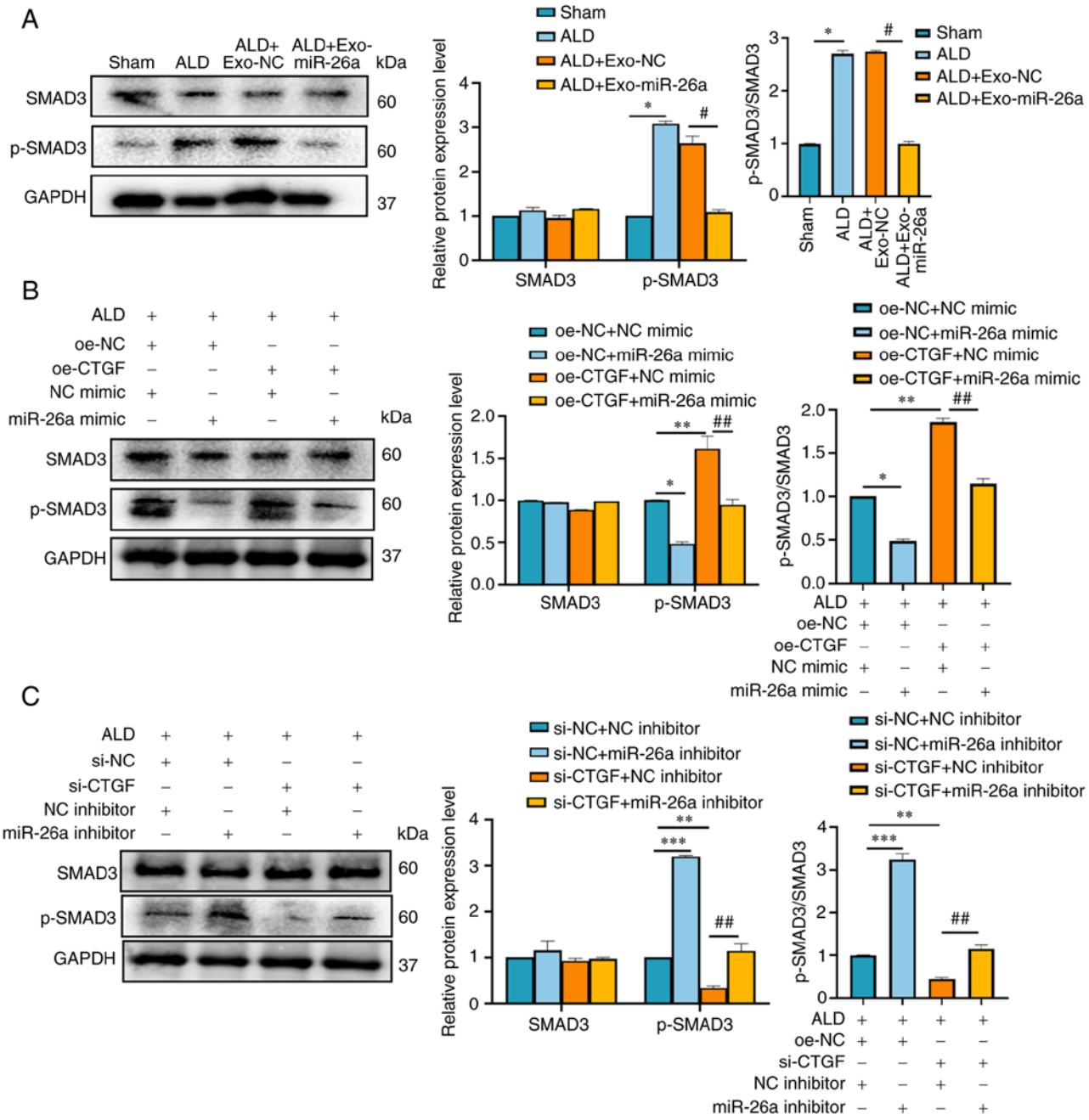

Figure 6. miR-26a/CTGF inhibits SMAD3 activation. (A) Western blot analysis of SMAD3 and p-SMAD3 protein expression levels in the kidneys of mice in the sham, ALD, ALD + Exo-NC and ALD + Exo-miR-26a groups. (B) Western blot analysis of SMAD3 and p-SMAD3 protein expression levels in mTECs co-transfected with oe-CTGF or oe-NC and miR-26a mimic or NC mimic for 6 h, and then treated with ALD ($1x10^{-6}$ M) for 48 h. (C) Western blot analysis of SMAD3 and p-SMAD3 protein levels in mTECs co-transfected with si-CTGF or si-NC and miR-26a inhibitor or NC inhibitor for 6 h, and then treated with ALD ($1x10^{-6}$ M) for 48 h. Data are presented as mean ± SD; Data are presented as the mean ± SD; *P<0.05, **P<0.01, ***P<0.001; $^{\#}$P<0.05, $^{\#\#}$P<0.01. ALD, aldosterone; CTGF, connective tissue growth factor; Exo, exosome encapsulated; miR, microRNA; mTEC, mouse tubular epithelial cells; NC, negative control; p-phosphorylated.

that miR-26a may attenuate TIF by inhibiting CTGF expression in mTECs.

CTGF knockdown alleviates ALD-induced EMT and ECM deposition in mTECs. To further elucidate the role of CTGF in EMT and ECM deposition, ALD-treated mTECs were transfected with si-CTGF. After transfection with si-CTGF, miR-26a expression increased (Fig. 5A). In addition, the results of RT-qPCR and western blot analysis revealed that the mRNA and protein expression levels, respectively, of collagen I, α-SMA and LCN2 were reduced in the ALD + si-CTGF group compared with those in the ALD group (Fig. 5B and C); the protein expression of CTGF showed the same trend (Fig. 5C), whereas the E-cadherin protein expression level was the opposite (Fig. 5C). Immunofluorescence results showed that CTGF knockdown resulted in decreased α-SMA expression levels in ALD-treated mTECs (Fig. 5D); the immunofluorescence NC shown in Fig. S2D exhibits no notable difference compared with control group in Fig. 5D. Collectively, these results indicated that CTGF knockdown

alleviates ALD-induced EMT and ECM deposition in mTECs.

miR-26a/CTGF axis inhibits SMAD3 activation. SMAD proteins have been reported to be associated with TIF, where SMAD3 plays a pathogenic role and SMAD2 and SMAD7 are protective (29). We hypothesized that miR-26a/CTGF might attenuate ALD-induced EMT and ECM deposition in mTECs by inhibiting SMAD3 activation. To test this, SMAD3 and p-SMAD3 protein expression levels were examined in the kidneys of ALD-treated mice. Western blot analysis revealed that p-SMAD3 expression in the ALD + Exo-NC group was higher compared with that in the ALD + Exo-miR-26a group, whereas the expression level of SMAD3 did not differ (Fig. 6A). *In vitro*, p-SMAD3 expression was increased in cells transfected with NC mimic and oe-CTGF plasmids compared with cells transfected with NC mimic and oe-NC plasmids, whereas it was decreased in cells transfected with oe-NC + miR-26a mimic compared with cells transfected with oe-NC + NC mimic and in cells transfected with oe-CTGF + miR-26a mimic compared with cells transfected with oe-CTGF + NC mimic (Fig. 6B); there was no difference in SMAD3 expression between the groups. These data suggested that miR-26a may inhibit and CTGF may increase SMAD3 activation.

To further explore the underlying mechanism, miR-26a inhibitor and CTGF siRNA were transfected into ALD-treated mTECs. Western blot analysis demonstrated that the expression of p-SMAD3 was reduced in cells transfected with si-CTGF + NC inhibitor compared with cells transfected with si-NC + NC inhibitor, whereas the expression was elevated in cells transfected with si-NC + miR-26a inhibitor compared with NC inhibitor and si-NC, and in cells transfected with si-CTGF + miR-26a inhibitor compared with cells transfected with si-CTGF + NC inhibitor (Fig. 6C); no obvious changes were observed in SMAD3 expression between the groups.

In summary, miR-26a may inhibit p-SMAD3 expression by binding to CTGF to rescue ALD-mediated TIF *in vivo*, as well as EMT and ECM deposition *in vitro*.

Discussion

TIF is a serious consequence of CKD, leading to disease progression to end-stage renal disease (30). In the present study, it was demonstrated that injection of miR-26a-rich exosomes through the tail vein in mice effectively alleviated ALD-induced TIF *in vivo*, and miR-26a mimic transfection rescued EMT and ECM deposition in mTECs *in vitro* by inhibiting the activation of the CTGF/SMAD signaling pathway. Results from this study may provide a potential avenue for the treatment of TIF in CKD using Exo-miR-26a.

ALD, a member of the RAAS, has been demonstrated to act on the heart, blood vessels and kidneys, and is reported to damage the cardiovascular and renal systems by promoting tissue inflammation, injury, glomerulosclerosis and interstitial fibrosis (31,32). Our previous studies have also confirmed that hyperaldosteronism promotes podocyte damage, glomerular sclerosis, renal tubular epithelial cell damage, renal interstitial inflammation and fibrosis (7-9). The present study demonstrated that ALD promotes the upregulation of α-SMA, collagen I and LCN2 and the downregulation of E-cadherin *in vivo* and *in vitro*. The increased expression of collagen I suggested the deposition of ECM in the tubulointerstitium. The increase in α-SMA, a hallmark of mature myofibroblasts (33), and LCN2, a crucial injury response factor (34), and the decrease in E-cadherin, a marker protein of tubular epithelium, indicated that EMT occurred in the kidney and mTECs.

Exosomes are an important and universal form of intercellular communication, and can mediate communication between organs (35). In addition, exosomes can be used as therapeutic carriers and serve as biomarkers to diagnose several diseases in a non-invasive manner (36). Our previous study demonstrated that Exo-miR-26a can not only prevent muscle atrophy and limit TIF in a mouse model of unilateral ureteral obstruction (UUO), but also attenuate skeletal muscle atrophy and ameliorate uremic cardiomyopathy in a 5/6 nephrectomy mouse model (14,37). The present study verified that exosomes can transport miR-26a into the kidney and rescue ALD-induced TIF using DiD fluorescence imaging experiments, indicating that exosomes may be an effective tool for delivering miRNA into the kidney.

Increasing evidence suggests that miR-26a is associated with the fibrosis process in various organs. For example, miR-26a was shown to inhibit EMT of lens epithelial cells and lens fibrosis in an injury-induced anterior subcapsular cataract (ASC) model and the mouse lens anterior capsular injury model *in vivo* and in a TGFβ2-induced ASC model *in vitro* (17). Another previous study reported that miR-26a overexpression can suppress cardiomyocyte apoptosis caused by ST-elevation myocardial infarction and oxygen-glucose deprivation, and it can ameliorate cardiac dysfunction and fibrosis in cardiac remodeling (38). Furthermore, miR-26a can alleviate fibrosis in hypertensive myocardial fibrosis (39), diabetic cardiomyopathy (40), and idiopathic pulmonary fibrosis (16). In addition, our previous studies have demonstrated that miR-26a can limit muscle atrophy and alleviate cardiomyopathy and TIF (14,37). The present study also revealed that miR-26a expression was reduced in the kidney of the ALD-treated mice and mTECs. By contrast, miR-26a overexpression rescued the expression levels of α-SMA, collagen I, CTGF and E-cadherin in ALD-induced mice and mTECs. These results suggested that increased miR-26a levels may serve an important role in alleviating TIF.

In addition, the present study verified that miR-26a targets CTGF to reduce its expression level. CTGF is mainly expressed and secreted by proximal tubular epithelial cells and renal interstitial fibroblasts in the kidney (41), and it is a pro-fibrotic factor involved in many chronic diseases. CTGF is involved in the fibrosis of various organ systems, including the liver, lungs, skin and kidneys (42,43). Increasing evidence shows that increased expression of CTGF in CKD kidney tissue is closely related to TIF (14,37,44). Our previous studies confirmed that CTGF was upregulated in the mouse model of UUO and 5/6 nephrectomy (14,37). The current study also revealed that CTGF was elevated in the ALD-treated mice. Moreover, in an experiment to verify the binding relationship between miR-26a and CTGF, the results showed that miR-26a expression is associated with CTGF expression, and vice versa. Given the above functions of CTGF, miR-26a may be an ideal factor to alleviate fibrosis, owing to its ability to inhibit the expression of CTGF.

SMAD protein family members are involved in organ fibrosis, and previous studies showed that deletion of SMAD3 inhibits renal fibrosis induced by almost all etiologies (45,46), and deletion of SMAD2 significantly enhances renal fibrosis (29), which indicates SMAD3 as a pathogenic protein. The present study revealed that p-SMAD3 expression in the kidneys of ALD-treated mice was increased compared with that in sham-treated mice, and the expression levels in the ALD + Exo-miR-26a mice were decreased compared with the ALD + Exo-NC mice. *In vitro*, miR-26a mimic and si-CTGF transfection alleviated EMT and ECM deposition in mTECs compared with miR-26a inhibitor and CTGF overexpression plasmids. These findings indicated that miR-26a restrained the activation of SMAD3 to rescue fibrosis.

In the present study, however, the expression status of miR-26a was not detected in tissues in TIF patients owing to the lack of tissue samples, which is an area of future research. Since injection through the tail vein is not targeted delivery, further experiment should be conducted to determine how to make exosomes able to target and transport miR-26a into the kidneys to achieve a better treatment plan. Owing to the different role of SMAD2 and SMAD3 in the regulation of pro-fibrotic TGF-β1 responses in human proximal-tubule epithelial cells, investigations into the role of SMAD2 and the regulatory relationship between SMAD2 and SMAD3 may increase our understanding of TGF-β1 in follow-up experiments.

In conclusion, the present study results demonstrated that the downregulation of miR-26a serves a significant role in the occurrence and development of TIF, and exosomes containing abundant miR-26a effectively alleviated TIF. These findings may provide us with a theoretical basis for the treatment of TIF.

Acknowledgements

Not applicable.

Funding

This work was supported by The National Natural Science Foundation of China (grant no. 81970664), The Natural Science Foundation of Jiangsu Province (grant no. BK2021022945), and the 789 Outstanding Talent Program of SAHNMU (grants nos. 789ZYRC202080119 and 789ZYRC202090251).

Availability of data and materials

The datasets used and/or analyzed during the current study are available from the corresponding author on reasonable request.

Authors' contributions

AZ designed the study. HZ and JJ performed the experiments and wrote the manuscript. TZ and EW contributed to the data analysis. HZ and JJ confirm the authenticity of all the raw data. All authors have read and approved the final manuscript.

Ethics approval and consent to participate

The experimental procedures in the present study were approved by Nanjing Medical University (Nanjing, China; ref. no. IACUC-2107049).

Patient consent for publication

Not applicable.

Competing interests

The authors declare that they have no competing interests.

References

1. GBD Chronic Kidney Disease Collaboration: Global, regional, and national burden of chronic kidney disease, 1990-2017: A systematic analysis for the global burden of disease study 2017. Lancet 395: 709-733, 2020.
2. Kramer H: Diet and chronic kidney disease. Adv Nutr 10 (Suppl 4): S367-S379, 2019.
3. Liyanage T, Toyama T, Hockham C, Ninomiya T, Perkovic V, Woodward M, Fukagawa M, Matsushita K, Praditpornsilpa K, Hooi LS, *et al*: Prevalence of chronic kidney disease in Asia: A systematic review and analysis. BMJ Glob Health 7: e007525, 2022.
4. Qi R and Yang C: Renal tubular epithelial cells: The neglected mediator of tubulointerstitial fibrosis after injury. Cell Death Dis 9: 1126, 2018.
5. Lerman LO: Imaging: BOLD assessment-effects of RAAS inhibition in CKD. Nat Rev Nephrol 10: 247-248, 2014.
6. Blasi ER, Rocha R, Rudolph AE, Blomme EAG, Polly ML and McMahon EG: Aldosterone/salt induces renal inflammation and fibrosis in hypertensive rats. Kidney Int 63: 1791-1800, 2003.
7. Yuan Y, Zhang A, Qi J, Wang H, Liu X, Zhao M, Duan S, Huang Z, Zhang C, Wu L, *et al*: p53/Drp1-dependent mitochondrial fission mediates aldosterone-induced podocyte injury and mitochondrial dysfunction. Am J Physiol Renal Physiol 314: F798-F808, 2018.
8. Shi H, Zhang A, He Y, Yang M and Gan W: Effects of p53 on aldosterone-induced mesangial cell apoptosis in vivo and in vitro. Mol Med Rep 13: 5102-5108, 2016.
9. Qu G, Shi H, Wang B, Li S, Zhang A and Gan W: Alterations in the long noncoding RNA transcriptome in mesangial cells treated with aldosterone in vitro. Mol Med Rep 16: 6004-6012, 2017.
10. Bartel DP: Metazoan MicroRNAs. Cell 173: 20-51, 2018.
11. Chandrasekaran K, Karolina DS, Sepramaniam S, Armugam A, Wintour EM, Bertram JF and Jeyaseelan K: Role of microRNAs in kidney homeostasis and disease. Kidney Int 81: 617-627, 2012.
12. Zheng Z, Guan M, Jia Y, Wang D, Pang R, Lv F, Xiao Z, Wang L, Zhang H and Xue Y: The coordinated roles of miR-26a and miR-30c in regulating TGFbeta1-induced epithelial-to-mesenchymal transition in diabetic nephropathy. Sci Rep 6: 37492, 2016.
13. Wang H, Wang B, Zhang A, Hassounah F, Seow Y, Wood M, Ma F, Klein JD, Price SR and Wang XH: Exosome-mediated miR-29 transfer reduces muscle atrophy and kidney fibrosis in mice. Mol Ther 27: 571-583, 2019.
14. Zhang A, Wang H, Wang B, Yuan Y, Klein JD and Wang XH: Exogenous miR-26a suppresses muscle wasting and renal fibrosis in obstructive kidney disease. FASEB J 33: 13590-13601, 2019.
15. Wei C, Kim IK, Kumar S, Jayasinghe S, Hong N, Castoldi G, Catalucci D, Jones WK and Gupta S: NF-kappaB mediated miR-26a regulation in cardiac fibrosis. J Cell Physiol 228: 1433-1442, 2013.
16. Kadota T, Fujita Y, Araya J, Watanabe N, Fujimoto S, Kawamoto H, Minagawa S, Hara H, Ohtsuka T, Yamamoto Y, *et al*: Human bronchial epithelial cell-derived extracellular vesicle therapy for pulmonary fibrosis via inhibition of TGF-beta-WNT crosstalk. J Extracell Vesicles 10: e12124, 2021.
17. Chen X, Xiao W, Chen W, Liu X, Wu M, Bo Q, Luo Y, Ye S, Cao Y and Liu Y: MicroRNA-26a and -26b inhibit lens fibrosis and cataract by negatively regulating Jagged-1/Notch signaling pathway. Cell Death Differ 24: 1431-1442, 2017.

18. Jiang S, Jiang W, Xu Y, Wang X, Mu Y and Liu P: Serum miR-21 and miR-26a levels negatively correlate with severity of cirrhosis in patients with chronic hepatitis B. Microrna 8: 86-92, 2019.
19. Smyth T, Kullberg M, Malik N, Smith-Jones P, Graner MW and Anchordoquy TJ: Biodistribution and delivery efficiency of unmodified tumor-derived exosomes. J Control Release 199: 145-155, 2015.
20. Mahtal N, Lenoir O, Tinel C, Anglicheau D and Tharaux PL: MicroRNAs in kidney injury and disease. Nat Rev Nephrol 18: 643-662, 2022.
21. Srivastava SP, Koya D and Kanasaki K: MicroRNAs in kidney fibrosis and diabetic nephropathy: Roles on EMT and EndMT. Biomed Res Int 2013: 125469, 2013.
22. Trionfini P, Benigni A and Remuzzi G: MicroRNAs in kidney physiology and disease. Nat Rev Nephrol 11: 23-33, 2015.
23. Colombo M, Raposo G and Thery C: Biogenesis, secretion, and intercellular interactions of exosomes and other extracellular vesicles. Annu Rev Cell Dev Biol 30: 255-289, 2014.
24. Skog J, Würdinger T, van Rijn S, Meijer DH, Gainche L, Sena-Esteves M, Curry WT Jr, Carter BS, Krichevsky AM and Breakefield XO: Glioblastoma microvesicles transport RNA and proteins that promote tumour growth and provide diagnostic biomarkers. Nat Cell Biol 10: 1470-1476, 2008.
25. Jalabert A, Vial G, Guay C, Wiklander OPB, Nordin JZ, Aswad H, Forterre A, Meugnier E, Pesenti S, Regazzi R, *et al*: Exosome-like vesicles released from lipid-induced insulin-resistant muscles modulate gene expression and proliferation of beta recipient cells in mice. Diabetologia 59: 1049-1058, 2016.
26. Vinas JL, Burger D, Zimpelmann J, Haneef R, Knoll W, Campbell P, Gutsol A, Carter A, Allan DS and Burns KD: Transfer of microRNA-486-5p from human endothelial colony forming cell-derived exosomes reduces ischemic kidney injury. Kidney Int 90: 1238-1250, 2016.
27. Livak KJ and Schmittgen TD: Analysis of relative gene expression data using real-time quantitative PCR and the 2(-Delta Delta C(T)) method. Methods 25: 402-408, 2001.
28. Liang H, Xu C, Pan Z, Zhang Y, Xu Z, Chen Y, Li T, Li X, Liu Y, Huangfu L, *et al*: The antifibrotic effects and mechanisms of microRNA-26a action in idiopathic pulmonary fibrosis. Mol Ther 22: 1122-1133, 2014.
29. Tang PM, Zhang YY, Mak TSK, Tang PCT, Huang XR and Lan HY: Transforming growth factor-beta signalling in renal fibrosis: From smads to non-coding RNAs. J Physiol 596: 3493-3503, 2018.
30. Li ZL and Liu BC: Hypoxia and renal tubulointerstitial fibrosis. Adv Exp Med Biol 1165: 467-485, 2019.
31. Epstein M: Aldosterone blockade: An emerging strategy for abrogating progressive renal disease. Am J Med 119: 912-919, 2006.
32. Hostetter TH and Ibrahim HN: Aldosterone in chronic kidney and cardiac disease. J Am Soc Nephrol 14: 2395-2401, 2003.
33. Shinde AV, Humeres C and Frangogiannis NG: The role of alpha-smooth muscle actin in fibroblast-mediated matrix contraction and remodeling. Biochim Biophys Acta Mol Basis Dis 1863: 298-309, 2017.
34. Rudman-Melnick V, Adam M, Potter A, Chokshi SM, Ma Q, Drake KA, Schuh MP, Kofron JM, Devarajan P and Potter SS: Single-cell profiling of AKI in a murine model reveals novel transcriptional signatures, profibrotic phenotype, and epithelial-to-stromal crosstalk. J Am Soc Nephrol 31: 2793-2814, 2020.
35. Shen AR, Zhong X, Tang TT, Wang C, Jing J, Liu BC and Lv LL: Integrin, exosome and kidney disease. Front Physiol 11: 627800, 2020.
36. Kalluri R and LeBleu VS: The biology, function, and biomedical applications of exosomes. Science 367: eaau6977, 2020.
37. Wang B, Zhang A, Wang H, Klein JD, Tan L, Wang ZM, Du J, Naqvi N, Liu BC and Wang XH: miR-26a limits muscle wasting and cardiac fibrosis through exosome-mediated microrna transfer in chronic kidney disease. Theranostics 9: 1864-1877, 2019.
38. Chiang MH, Liang CJ, Lin LC, Yang YF, Huang CC, Chen YH, Kao HL, Chen YC, Ke SR and Lee CW: miR-26a attenuates cardiac apoptosis and fibrosis by targeting ataxia-telangiectasia mutated in myocardial infarction. J Cell Physiol 235: 6085-6102, 2020.
39. Zhang W, Wang Q, Feng Y, Chen X, Yang L, Xu M, Wang X, Li W, Niu X and Gao D: MicroRNA-26a protects the heart against hypertension-induced myocardial fibrosis. J Am Heart Assoc 9: e017970, 2020.
40. Zhu C, Zhang H, Wei D and Sun Z: Silencing lncRNA GAS5 alleviates apoptosis and fibrosis in diabetic cardiomyopathy by targeting miR-26a/b-5p. Acta Diabetol 58: 1491-1501, 2021.
41. Ito Y, Aten J, Bende RJ, Oemar BS, Rabelink TJ, Weening JJ and Goldschmeding R: Expression of connective tissue growth factor in human renal fibrosis. Kidney Int 53: 853-861, 1998.
42. Perbal B: CCN proteins: Multifunctional signalling regulators. Lancet 363: 62-64, 2004.
43. Wang S, Denichilo M, Brubaker C and Hirschberg R: Connective tissue growth factor in tubulointerstitial injury of diabetic nephropathy. Kidney Int 60: 96-105, 2001.
44. Okada H, Kikuta T, Kobayashi T, Inoue T, Kanno Y, Takigawa M, Sugaya T, Kopp JB and Suzuki H: Connective tissue growth factor expressed in tubular epithelium plays a pivotal role in renal fibrogenesis. J Am Soc Nephrol 16: 133-143, 2005.
45. Lan HY: Transforming growth factor-beta/Smad signalling in diabetic nephropathy. Clin Exp Pharmacol Physiol 39: 731-738, 2012.
46. Sato M, Muragaki Y, Saika S, Roberts AB and Ooshima A: Targeted disruption of TGF-beta1/Smad3 signaling protects against renal tubulointerstitial fibrosis induced by unilateral ureteral obstruction. J Clin Invest 112: 1486-1494, 2003.